

Sedimentation of homogeneous suspensions of non-Brownian spheres

Anthony J. C. Ladd

Lawrence Livermore National Laboratory, Livermore, California 94550

(Received 12 September 1996; accepted 13 November 1996)

Dynamical simulations of bulk sedimentation have been carried out, using up to 32 000 solid particles. There is no evidence that the long-range hydrodynamic interactions are screened by changes in the pair correlation function at large distances. Instead the velocity fluctuations and diffusion coefficients diverge linearly with the width of the container, consistent with the random long-range microstructures observed in the simulations. Our data suggest that other mechanisms must be uncovered to account for experimental observations. © 1997 American Institute of Physics. [S1070-6631(97)02403-3]

I. INTRODUCTION

An isolated sphere of macroscopic size falls steadily through a suspending liquid, at a terminal velocity, U_0 , set by the balance between the gravitational force and the hydrodynamic or Stokes drag. In a multi-particle suspension each particle experiences a different shielding of the hydrodynamic drag, due to fluctuating arrangements of its neighbors. These solvent mediated “hydrodynamic interactions” are long range, decaying as $1/R$ at large particle separations (R). They drive fluctuations in particle velocity during the sedimentation process, which leads to a diffusive motion of the particles in addition to the net sedimentation flow. The root-mean-square fluctuations in particle velocity are of the same magnitude as the mean sedimentation velocity; for particles more than about $10 \mu\text{m}$ in diameter, hydrodynamic diffusion completely dominates the thermal Brownian motion. A straightforward calculation shows that particle velocity fluctuations in a suspension of randomly distributed particles diverge in the large system limit.¹ On the other hand, recent experiments found no systematic variation in the particle velocity fluctuations with container size.² These theoretical and experimental findings raise the question as to whether velocity fluctuations in sedimenting suspensions are controlled by the container size, by the establishment of a non-random suspension microstructure, or by some mechanism which has not yet been considered.

It has been suggested that changes in long-range pair correlations, induced by the sedimentation process, might lead to a screening of the hydrodynamic interactions.³ If the long-range interactions are screened, then velocity fluctuations in sedimenting suspensions would be finite and independent of container size for sufficiently large vessels. The critical test of this theory is its prediction of a mass deficit; in other words that the neighborhood around a test sphere contains precisely one less particle than if the same volume were filled uniformly with particles at the bulk suspension concentration. This prediction has not been tested experimentally since the particles used in the laboratory are too large to allow for a direct measurement of the structure factor by light scattering. Thus numerical simulation is the only technique presently available to study the microstructure (pair correlations) in sedimenting suspensions and to test for a mass deficit. The motivation for this work was to discover if

hydrodynamic screening occurs in uniform sedimenting suspensions, in the absence of inhomogeneities introduced by cell boundaries. A preliminary account of this work was published recently.⁴

II. HYDRODYNAMIC FLUCTUATIONS

In a typical sedimentation experiment the particle Reynolds number is of order 10^{-4} .^{2,5,6} Thus both particle inertia and fluid inertia can be ignored and the velocity of a particle is completely determined by the instantaneous configuration of its neighbors;

$$\mathbf{U}_i = \sum_{j=1}^N \boldsymbol{\mu}_{ij}(\mathbf{R}^N) \cdot \mathbf{F}, \quad (1)$$

where $\boldsymbol{\mu}_{ij}(\mathbf{R}^N)$ are the configuration dependent mobility matrices, and \mathbf{F} is the gravitational force on each of the (identical) spheres. In addition to the direct hydrodynamic interactions between the spheres, there is a pressure gradient, generated by the base of the container, which exactly balances the total gravitational force on the particles; i.e.,

$$\int_V \nabla p(\mathbf{r}) d\mathbf{r} = N\mathbf{F}, \quad (2)$$

where N is the number of spheres in the sample volume V . On average, the backflow of fluid induced by this pressure gradient cancels the contributions of the hydrodynamic interactions at large distances, so that the mean sedimentation velocity is finite and independent of container size⁷ and shape.⁸ However, *fluctuations* in particle velocity,

$$\langle \mathbf{U}_i \mathbf{U}_i \rangle = \left\langle \sum_{j=1}^N \sum_{k=1}^N \mathbf{F} \cdot \boldsymbol{\mu}_{ij}(\mathbf{R}^N) \boldsymbol{\mu}_{ik}(\mathbf{R}^N) \cdot \mathbf{F} \right\rangle, \quad (3)$$

are not affected by the backflow. The contributions of distant particles to the velocity variance of a test sphere fall off as R^{-2} ; when summed over all particles in the system (apart from the test sphere), they give a contribution to the velocity variance that is proportional to the linear dimensions of the container.¹ For a sample with periodic boundary conditions, the *diverging* contribution to the velocity fluctuations can be written in a simpler form as a sum over wave vectors, \mathbf{k} , that are commensurate with the periodic box,⁹

$$\langle \mathbf{U}\mathbf{U} \rangle = \frac{N}{V^2} \sum_{\mathbf{k} \neq 0} S(\mathbf{k}) \mathbf{F} \cdot \mathbf{T}(\mathbf{k}) \mathbf{T}(\mathbf{k}) \cdot \mathbf{F}. \quad (4)$$

In this equation $S(\mathbf{k}) = \langle N^{-1} \sum_{i,j=1}^N e^{i\mathbf{k} \cdot \mathbf{R}_{ij}} \rangle$ is the structure factor, which is direction dependent because of the gravitational field; $\mathbf{T}(\mathbf{k}) = (\mathbf{1} - \mathbf{k}\mathbf{k}/k^2)/\eta k^2$ is the periodic Green's function for hydrodynamic interactions in a fluid of viscosity η . The $\mathbf{k} = 0$ term is canceled by the pressure gradient [Eq. (2)].

At long wavelengths,

$$S(\mathbf{k}) = S(0) + \mathcal{O}(k^2); \quad (5)$$

thus only the long wavelength limit $S(0)$ contributes to the divergence of $\langle \mathbf{U}\mathbf{U} \rangle$. The velocity fluctuations can then be written in terms of the volume fraction, ϕ , and the ratio of the sample width, W , to the particle radius, a ,

$$\langle U_\alpha^2 \rangle = C_\alpha \phi U_0^2 S(0) W/a; \quad (6)$$

the label α refers to fluctuations parallel or perpendicular to the gravitational field and C_α is a numerical coefficient which depends on the box shape. For elongated boxes, Eq. (4) can be simplified by replacing the sum over the component of \mathbf{k} parallel to the gravitational direction by an integral. Then it is straightforward to calculate the coefficients C_α , with the result

$$C_{\parallel} = 10C_{\perp} = \frac{135}{256\pi^2} \sum_{\mathbf{n} \neq 0} n^{-3} = 0.48268; \quad (7)$$

the summation is over the two-dimensional space $\mathbf{n} = [n_x, n_y]$.

The divergence in the velocity variance, proportional to W/a , is directly connected to the behavior of long wavelength density fluctuations, described by $S(k)$ in the limit $k \rightarrow 0$. If particle positions are uncorrelated beyond a few sphere diameters, then $S(0)$ is finite and the velocity fluctuations diverge. If, on the other hand, long-wavelength density fluctuations are for some reason suppressed, and $S(0) = 0$, then the velocity fluctuations will be finite,³ even for very large samples. An analogous situation occurs in electrolyte solutions, where long-wavelength fluctuations in charge density are suppressed by Debye–Hückel screening. The charges rearrange so that an ion and its environment are overall electrically neutral on length scales greater than the Debye–Hückel screening length. Thus in charged systems there are long-range pair correlations (on the order of the screening length), which are such that the charge–charge structure factor vanishes in the long-wavelength limit. Koch and Shaqfeh³ have proposed that a similar mechanism could suppress the velocity fluctuations in sedimenting suspensions. Here the pressure gradient in the background fluid plays the same role as the counterions in an electrolyte solution. The equivalent Koch–Shaqfeh screening of the hydrodynamic interactions requires that a sedimenting sphere and its neighbors are neutrally buoyant with respect to the homogeneous suspension. In terms of the pair correlation function, $g(\mathbf{r}) = \langle N^{-1} \sum_{i \neq j=1}^N \delta(\mathbf{r} - \mathbf{R}_{ij}) \rangle$, hydrodynamic screening requires that

$$\frac{N}{V} \int_{V_\lambda} [g(\mathbf{r}) - 1] d\mathbf{r} = -1. \quad (8)$$

The integral in Eq. (8) is over a spherical volume of radius λ , where λ is much greater than the particle radius a but much less than the (macroscopic) size of the container. Thus for hydrodynamic screening to occur, the number of neighbors in a *submacroscopic* volume around a test sphere, V_λ , must be exactly one particle less than if that same volume were filled uniformly with particles.³ Using the relation between the structure factor and the pair correlation function, $S(\mathbf{k}) = 1 + (N/V) \int \cos(\mathbf{k} \cdot \mathbf{r}) [g(\mathbf{r}) - 1] d\mathbf{r}$, it is clear that Eq. (8) is equivalent to the condition $S(0) = 0$.

Recent laboratory experiments have studied the variation in particle velocity fluctuations with container size.² No systematic changes in velocity variance were observed over a range of container widths, W , from $50a$ to $200a$. The motivation for the present work was to discover whether this experimental observation can be explained by a hydrodynamic screening mechanism, along the lines proposed by Koch and Shaqfeh.³ This has been accomplished by large-scale numerical simulations, which allow us to measure both the velocity fluctuations and the pair correlation functions.⁴ In this work, more than 32 000 spheres have been simulated; the largest box width is about $70a$, in the same range as the laboratory experiments, and much larger than the predicted screening length in the Koch–Shaqfeh theory, which suggests $\lambda \approx a/\phi$. To minimize the expected screening length, while still keeping the suspension reasonably dilute, most simulations were run at a volume fraction $\phi = 0.1$. A wide range of system sizes, from $N = 128$ to $N = 32\,768$, were used, to compare the scaling of the velocity fluctuations with the predictions of Eq. (6) for random long-range microstructures, and with the predictions of Ref. 3 for screened hydrodynamic interactions.

III. NUMERICAL METHOD

The numerical method used in this work is similar to that described in Ref. 10: the fluid phase is described by a lattice-Boltzmann model which interacts with the solid particles at special “boundary nodes” on the particle surfaces; the solid particle motion is calculated by molecular dynamics. The accuracy of the lattice-Boltzmann approach was established by extensive comparisons with theory, simulation, and experiment.¹¹ However, due to the added complexities involved in combining dynamical simulations with a parallel implementation of the code, it was necessary to modify the method in two important respects. Several of the key numerical tests described in Ref. 11 have been repeated for the modified method and are reported below. Once again we use a system of units in which the nearest-neighbor lattice spacing and the time step are both unity.

In the original implementation particle centers were always located at lattice nodes, which maintains a fixed particle shape. However, during a dynamical simulation it is then necessary to move the particle in discrete steps, corresponding to motion from lattice node to lattice node. Unfortunately this leads to “traffic jams,” even in relatively dilute suspensions, with particles waiting to move to the correct

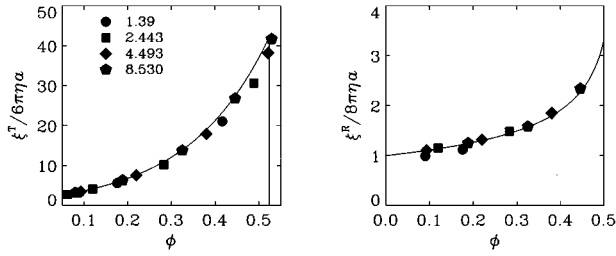


FIG. 1. Translational and rotational friction coefficients of a simple-cubic lattice of spheres. The drag coefficients, normalized by the isolated sphere values, are plotted as a function of volume fraction for several different size objects. The solid lines are determined from accurate numerical solutions of the Stokes equations.¹⁵

locations. A further disadvantage is that when a particle moves it causes noticeable discontinuities in the fluid flow. Thus in this work the particles move continuously, using the instantaneous particle coordinates as the center for the map of boundary nodes.¹² The disadvantage of this approach is that the particle shape fluctuates as the location of the particle changes with respect to the lattice; however, the fluctuations in shape are insignificant for sphere radii greater than about 5 lattice spacings. When an object has its center located at a lattice node, the two methods produce identical drag coefficients.

In order to determine the effective hydrodynamic radius of an object, the mean friction coefficient of a periodic array of spheres was measured at low volume fraction ($\phi < 0.1$). The method is similar to that described in Ref. 11, except that it is now necessary to average over an ensemble of different particle locations (relative to the lattice). One hundred randomly chosen locations were used for each test, even though there was very little variation in drag for larger objects. It was found that for input radii of 1.5, 2.5, 4.5, and 8.5 lattice spacings, the effective hydrodynamic radii, based on the mean friction coefficients, were 1.39, 2.443, 4.493, and 8.530, respectively. The effective hydrodynamic radius is used to estimate the solid volume fraction of a suspension.

The translational and rotational friction coefficients for a simple-cubic array of spheres are shown as a function of solid volume fraction in Fig. 1 (cf. Fig. 2 of Ref. 11); each data point was obtained by an ensemble average over 100 different particle locations. The simulation data are in good agreement with creeping-flow theory over the whole range of volume fraction.

It is possible for two particles near contact to share the same boundary node. In such cases a special update rule is needed for these “shared nodes.” The update rule used in Ref. 11 is particularly cumbersome in parallel implementations. Therefore population densities now simply propagate through shared nodes undisturbed, as in the bulk fluid. In addition the leading order lubrication forces are calculated explicitly:

$$\mathbf{F}_{ij}^{lub} = -\frac{3\pi\eta a}{s} \hat{\mathbf{x}}_{ij} \hat{\mathbf{x}}_{ij} \cdot (\mathbf{u}_i - \mathbf{u}_j), \quad (9)$$

where $s = R/a - 2$ is the dimensionless gap and $\mathbf{x}_{ij} = \mathbf{x}_i - \mathbf{x}_j$. The lattice-Boltzmann method breaks down

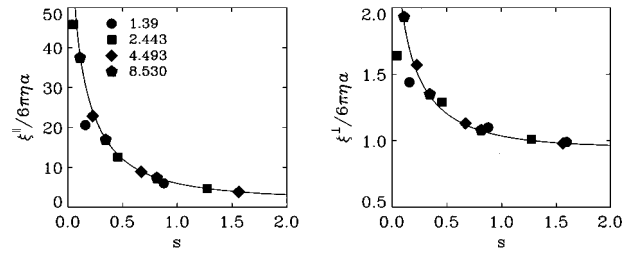


FIG. 2. Hydrodynamic interactions between pairs of spheres. The perpendicular and parallel friction coefficients are plotted as a function of the reduced gap width, $s = R/a - 2$. The systems are periodic, with a two-sphere unit cell. The solid lines are solutions of the Stokes equations,¹⁵ in the same periodic geometry.

when the particles are closer than some separation Δ , where Δ is of the order of one lattice spacing. Thus the missing lubrication can be accounted for by taking the difference in lubrication force between $R = (2+s)a$ and $R = 2a + \Delta$ for each closely spaced pair ($R < 2a + \Delta$); in other words by replacing $1/s$ in Eq. (9) with $1/s - a/\Delta$. The pair hydrodynamic interactions calculated in this way are illustrated in Fig. 2 (cf. Fig. 3 of Ref. 11), taking $\Delta = 1$.

Calculations of hydrodynamic transport coefficients for random dispersions have also been repeated; the results for periodic unit cells containing 16 spheres are shown in Fig. 3 (cf. Fig. 4 of Ref. 11). The shear viscosity is in better agreement with creeping-flow theory than in Ref. 11, because of the explicit lubrication forces. The overall agreement between lattice-Boltzmann results and creeping-flow theory, illustrated in Figs. 1–3, is quite comparable to observations in Ref. 11.

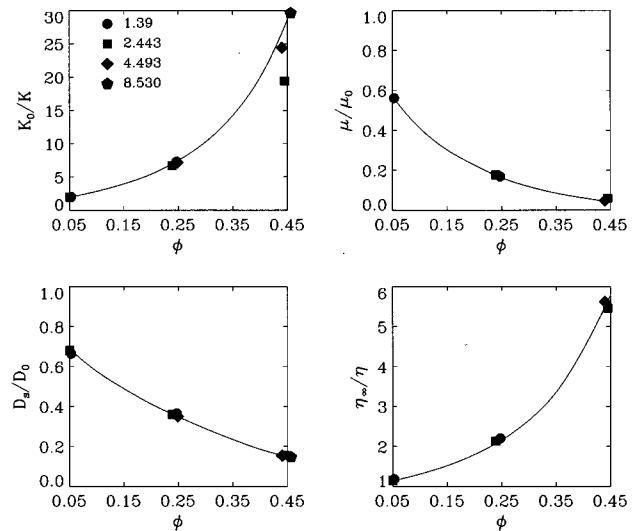


FIG. 3. Hydrodynamic transport coefficients of random arrays of spheres. The inverse permeability, K^{-1} , the collective mobility, μ , the self diffusion coefficient, D_s , and the high frequency shear viscosity, η_∞ , have been normalized to the appropriate low-density limit. Results from simulations of 16 spheres (with periodic boundary conditions) are compared with accurate numerical solutions of the Stokes equations. The lattice-Boltzmann results (present work) are plotted as symbols; results from Ref. 16 are shown as solid lines. The statistical errors in both sets of calculations are smaller than the plotting symbols.

A parallel version of the code was implemented, first for the Meiko CS2 and later for the IBM SP2. The code used a two-dimensional domain decomposition of the fluid, but for simplicity, the dynamics of the solid particles were solved on every processor. The algorithm parallelizes quite efficiently for as many as 10 000 particles, using up to 64 processors. For very large systems, the absence of a parallel code for the solid particles reduces the efficiency; systems of more than 100, 000 particles are not feasible without parallelization of the particle dynamics. In the present work, 32 processors were used for the largest calculations. On the IBM SP2 this gave a total performance of about 2 Gflops, or about 5 million site updates per second.

IV. RESULTS

The principal aim of this work has been to discover whether or not hydrodynamic screening exists in bulk sedimentation of non-Brownian spheres. The primary data obtained from the simulations have been the particle velocity fluctuations and pair correlation functions. The scaling of velocity fluctuations has been examined over a large range of system sizes, from $N \approx 100$ to $N \approx 32\,000$, to see if it is consistent with random long-range microstructures, or whether the fluctuations tend to constant values for sufficiently large systems, indicating hydrodynamic screening. More directly, pair correlation functions have been examined for evidence of hydrodynamic screening.

There is a source of uncertainty in the simulations, arising from fluctuations in shape as the particles move through the lattice (see Sec. III). Thus an isolated pair of spheres has an artificial tendency to separate during sedimentation. However, the rate of separation in several two-particle test calculations was found to be small, and decreasing in proportion to the particle size. For the smallest spheres ($a = 1.39$), the average rate of divergence of particle trajectories is less than 1% of the Stokes velocity; for larger particles ($a = 2.443$) the rate of divergence is less than 0.5%. By comparison, the experimental data suffer from direct polydispersity effects that are at least an order of magnitude larger.

In addition to the various tests for static arrays of particles discussed in Sec. III and in Ref. 11, some additional calculations were undertaken to specifically validate the simulation method for the sedimentation problem; these include the effects of a shear flow on the relative velocity of a pair of spheres (Sec. IV A), and comparisons with previous dynamical simulations (Sec. IV B). Simulations in elongated boxes have been carried out to assess the effects of box *shape* and to help decide on the most useful aspect ratio for the later simulations (Sec. IV C). The bulk of the new results are described in the two subsequent sections (Sec. IV D and IV E): velocity fluctuations, time-dependent velocity correlations, and particle–particle spatial correlations are compared with theoretical predictions and experimental results. The emphasis of this work is on scaling of the velocity fluctuations and on the long-range behavior of the pair correlation function.

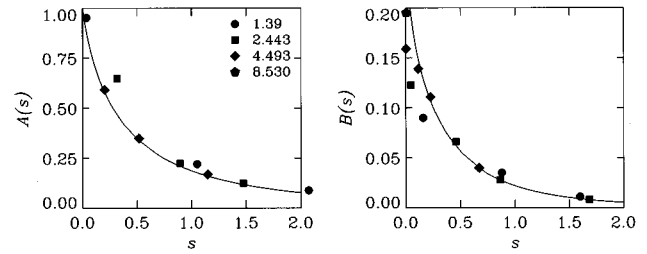


FIG. 4. Velocities of a pair of spheres in shear flow. The scalar coefficients A and B that characterize the relative motion of the spheres are compared with Batchelor and Green's results (solid lines).¹³ Simulation results are plotted as a function of the reduced gap width, $s = r/a - 2$, for various particle sizes.

A. A pair of spheres in a shear flow

An important element of the Koch–Shaqfeh theory³ is that the relative positions of a closely spaced pair of particles are modified by the shear-flow induced by a distant third particle. To ensure that these three-body interactions are simulated correctly, the velocities of a pair of spheres in a shear flow have been calculated. In these simulations the shear is induced by a pair of plane walls, rather than by a distant particle. The relative velocity $\mathbf{U} = \mathbf{U}_2 - \mathbf{U}_1$ of an isolated pair of spheres in a homogeneous shear flow is given by¹³

$$\mathbf{U} = \boldsymbol{\Omega} \times \mathbf{R} + \mathbf{E} \cdot \mathbf{R} - [A(R)\hat{\mathbf{R}}\hat{\mathbf{R}} + B(R)(\mathbf{1} - \hat{\mathbf{R}}\hat{\mathbf{R}})] \cdot \mathbf{E} \cdot \mathbf{R}, \quad (10)$$

where $\mathbf{R} = \mathbf{R}_2 - \mathbf{R}_1$ is the separation vector, and \mathbf{E} and $\boldsymbol{\Omega}$ are the strain rate and vorticity of the imposed shear flow. The scalar coefficients A and B can be determined by measuring the velocity of a pair of spheres at various orientations with respect to the flow. Three different orientations in the shear-flow plane were used; with the pair aligned along the flow direction, with the pair at right angles to the flow direction, and with the pair at 45° to the flow direction. These simulations provide two independent measurements for both A and B . Since the imposed flow is not exactly homogeneous but depends on the distance from the spheres to the driving walls, each sphere configuration was run with three different box sizes to estimate size effects. For the 45° configuration, the two measures of A (from the two different velocity components) converged quite rapidly, one from above and the other from below; thus a bounded estimate of A could be made, even for quite large spheres. For the B coefficient, it was difficult to get a convergent result from the case where the spheres were aligned along the flow direction; this arrangement was only useful for small, closely spaced spheres. The perpendicular arrangement showed much better convergence and was used for most of the calculations of B . A summary of the results is shown in Fig. 4, where the best estimates of A and B are plotted for various particle sizes as a function of the reduced gap, $s = R/a - 2$; Batchelor and Green's results¹³ are indicated by the solid lines. It can be seen that the A coefficient is accurately calculated at all separations, regardless of sphere size; this is because the small s behavior is captured by the explicit lubrication [Eq. (9)]. The small s behavior of the B coefficient is only captured

TABLE I. Comparison of simulated velocity fluctuations and hydrodynamic diffusion coefficients with Stokesian dynamics results. Simulations of 32 spheres in a cubic periodic box are compared with earlier results⁹ obtained by numerical solutions of creeping-flow integral equations (SD). Results are reported for different values of the Reynolds number, $R_W = \langle U_{\parallel} \rangle W / \nu$, which is based on the width of the periodic unit cell W .

a	ϕ	R_W	$\langle U_{\parallel} \rangle / U_0$	$\langle U_{\parallel}^2 \rangle / U_0^2$	$\langle U_{\perp}^2 \rangle / U_0^2$	$D_{\parallel} / U_0 a$	$D_{\perp} / U_0 a$
1.39	0.052	1.37	0.632	0.074	0.0061	3.6	0.053
		0.69	0.631	0.077	0.0067	3.4	0.051
		0.34	0.629	0.077	0.0067	3.9	0.046
		0.17	0.630	0.075	0.0066	3.5	0.045
SD	0.05	0.0	0.63	0.072	0.0069	3.5	0.054
1.39	0.107	0.37	0.426	0.045	0.0055	1.35	0.034
2.443	0.099	0.29	0.441	0.046	0.0057	1.35	0.035
2.443	0.244	0.38	0.197	0.016	0.0028	0.24	0.013
		0.19	0.194	0.015	0.0028	0.24	0.014
SD	0.25	0.0	0.19	0.015	0.0024	0.31	0.018

approximately, because the tangential lubrication has not been explicitly included. Nevertheless, the overall agreement is quite acceptable; the average motion of pair of spheres in a shear flow is accurately reproduced.

B. Comparison with previous results

Sedimentation simulations for 32 spheres in a cubic periodic box have been carried out, to compare the lattice-Boltzmann code with simulations based on a Stokesian dynamics like method.⁹ The results for velocity fluctuations and diffusion coefficients, ensemble-averaged over 64 different initial configurations, are collected in Table I; the statistical errors are of the order of 5%. Since the fluid equations in lattice-Boltzmann simulations are time dependent, the results depend on the mean particle velocity. Each simulation can be characterized by a Reynolds number,

$$R_W = \langle U_{\parallel} \rangle W / \nu, \quad (11)$$

based on the width of the cell W and the mean flow velocity $\langle U_{\parallel} \rangle$. The Reynolds number is a measure of the distance over which the hydrodynamic interactions spread before a particle moves a significant fraction of that distance; in this work it is based on the cell width so that the range of the hydrodynamic interactions increases in proportion to the cell size. Table I shows how the velocity fluctuations and diffusion coefficients vary with the mean flow velocity, as characterized by R_W . There is no systematic variation in either the velocity fluctuations or the diffusion coefficients for $R_W < 1$. In the simulations reported later in the paper $R_W \approx 0.4$; as the systems get larger the gravitational force is reduced in proportion, so as to keep R_W roughly constant. By comparison, in laboratory experiments $R_W \approx 0.03$, roughly a factor of 10 less.

The overall agreement between Stokesian dynamics and lattice-Boltzmann simulations is within 5% for the velocity fluctuations and 20% for the diffusion coefficients. Although these differences are not much larger than the combined statistical errors in the two calculations, the diffusion coefficients measured in the Stokesian dynamics simulations are

TABLE II. Box shape dependence of velocity fluctuations and hydrodynamic diffusion coefficients. Simulations in oblong periodic boxes of different aspect ratios H/W are compared. In all cases the effective hydrodynamic radius was 1.39 lattice spacings, the volume fraction $\phi = 0.107$, and $R_W = \langle U_{\parallel} \rangle W / \nu = 0.37$.

H/W	N	$\langle U_{\parallel} \rangle / U_0$	$\langle U_{\parallel}^2 \rangle / U_0^2$	$\langle U_{\perp}^2 \rangle / U_0^2$	$D_{\parallel} / U_0 a$	$D_{\perp} / U_0 a$
1	32	0.426	0.045	0.0055	1.35	0.034
2	64	0.429	0.041	0.0070	0.80	0.045
4	128	0.433	0.045	0.0072	0.62	0.040
8	256	0.427	0.042	0.0069	0.53	0.039
16	512	0.429	0.042	0.0071	0.59	0.043

consistently larger than those measured in the lattice-Boltzmann simulations. Since the static properties determined by both methods are very similar, the discrepancy is most likely due to the integration of the dynamical trajectories. In the Stokesian dynamics simulations, a time step equal to the Stokes time ($t_0 = a / U_0$) was used, which saved computer time but at the cost of a relatively large number of particle-particle contacts; this may have led to an overestimate of the dispersion coefficients. In this work the time step for particle motion is much smaller, at most $10^{-2} t_0$. Stokesian dynamics simulations are not available at 10% volume fraction, but the results of lattice-Boltzmann simulations with two different particle sizes are very similar.

C. Box shape effects

Somewhat surprisingly, it turns out that hydrodynamic diffusion is affected by box shape as well as box size. In earlier sedimentation simulations⁹ large anisotropies in the diffusion coefficients were found; at low volume fractions ($\phi = 0.05$) $D_{\parallel} / D_{\perp}$ was ≈ 65 . Subsequent experimental measurements found much smaller anisotropies; typical values of $D_{\parallel} / D_{\perp}$ ranged from about 5 at low volume fractions to about 3 at high volume fractions. A theoretical analysis¹⁴ indicates that this is at least partially due to the box shape. Using a self-consistent diffusion model for the particle motion, Koch¹⁴ showed that horizontal density fluctuations can be convected through the periodic repeat length before decaying due to particle diffusion. However, the anisotropy in velocity fluctuations and hydrodynamic diffusion coefficients is significantly reduced if the box is elongated in the direction of the gravitational field. The asymptotic aspect ratio is predicted to be about 4:1;¹⁴ no significant changes in velocity fluctuations or diffusion coefficients are expected for larger aspect ratios. In this work we have made a sequence of runs with different aspect ratios, varying from 1:1 to 16:1; velocity fluctuations and diffusion coefficients at a volume fraction $\phi = 0.1$ are reported in Table II.

The results in Table II show that the cubic box ($N = 32$) is significantly anomalous when compared with more elongated box shapes; fluctuations in the vertical direction are slightly enhanced and those in the horizontal direction are suppressed. The anisotropy is larger for the diffusion coefficients than for the instantaneous velocity fluctuations; thus the relaxation times are also shape dependent. The ratio of $D_{\parallel} / D_{\perp}$ ranges from 40 for $H/W = 1$ to about 14 for $H/W \geq 4$. However, even these anisotropies are much larger

TABLE III. Box size dependence of velocity fluctuations and hydrodynamic diffusion coefficients. Simulations in different size periodic boxes (with aspect ratio $H/W=4$) are compared. The number of particles in these simulations range from 128 to 32 768. Results for different size spheres at a volume fraction close to $\phi=0.1$ are shown. The applied force on each particle is set to keep R_w approximately constant for the different system sizes.

N	a	ϕ	R_w	$\langle U_{\parallel} \rangle / U_0$	$\langle U_{\parallel}^2 \rangle / U_0^2$	$\langle U_{\perp}^2 \rangle / U_0^2$	$D_{\parallel} / U_0 a$	$D_{\perp} / U_0 a$
128	1.39	0.107	0.37	0.433	0.045	0.0072	0.62	0.040
	2.443	0.099	0.40	0.454	0.050	0.0080	0.75	0.045
	4.493	0.097	0.41	0.462	0.050	0.0079	0.78	0.046
1024	1.39	0.107	0.41	0.482	0.148	0.0222	3.5	0.14
	2.443	0.099	0.45	0.508	0.168	0.0238	3.1	0.14
8192	1.39	0.107	0.44	0.507	0.388	0.0503	11.1	0.45
	7424	2.443	0.101	0.532	0.378	0.0546	9.8	0.45
32 768	1.39	0.107	0.45	0.517	0.599	0.0796	17.7	0.77

than the experimental results.⁶ In the next section we examine how hydrodynamic diffusion coefficients vary with system size and make more detailed comparisons with experiment.

D. Box size effects

Simulation results for velocity fluctuations and hydrodynamic diffusion coefficients are summarized in Table III for a range of system sizes from 128 to 32 768 spheres; in each case the aspect ratio of the unit cell was 4:1. In Fig. 5 velocity fluctuations are plotted as a function of the periodic repeat width W . It can be seen that the fluctuations diverge approximately linearly with W in accordance with the predictions of Eq. (6). The actual numerical values for the RMS velocity fluctuations are about one half the theoretical values for an equilibrium (most probable) distribution of spheres. The volume fraction used in the simulations ($\phi=0.1$) is probably too large for Eq. (4) to be more than qualitatively correct. The more quantitative agreement between theory and simulation reported in Ref. 4 was erroneous; a factor of π was inadvertently omitted from the theoretical calculation.

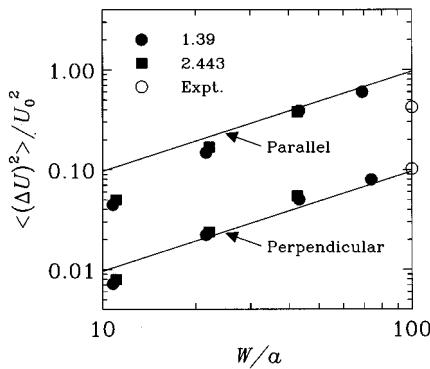


FIG. 5. Variation in velocity fluctuations with box size in a steadily sedimenting suspension. The solid line is the theoretical scaling ($\propto W$) for an equilibrium (most probable) distribution of spheres. Simulation results for two different particle sizes are shown, with hydrodynamic radii $a=1.39$ and $a=2.443$. Experimental results at a volume fraction $\phi=0.1$ are shown (as open symbols) for comparison.

Figure 5 contains results for two different particle sizes ($a=1.39$ and $a=2.443$); the data indicate that the divergence of the velocity fluctuations is independent of the particle radius used in the lattice-Boltzmann simulations. Furthermore, an additional simulation was performed with a larger particle ($a=4.5$) and these results (for $N=128$) also agreed with the smaller particle data (see Table III). Thus it would not be expected that more accurate simulations would lead to qualitatively different conclusions.

The simulations show that macroscopically homogeneous suspensions experience a divergence in the velocity fluctuations as W/a becomes large, as predicted by Caflich and Luke;¹ the fluctuations do not converge to a fixed value for sufficiently large systems, as predicted by Koch and Shaqfeh.³ Since the experimental systems are never perfectly homogeneous and the actual particle distribution is unknown, the experimental observations are not a definitive answer to the question as to whether screening can arise in a bulk suspension, as opposed to being caused by large scale inhomogeneities induced by the container. In these simulations the largest cell width ($W=70a$, $N=32\,768$) is of comparable dimensions to experimental cells in which no divergence in velocity fluctuations was observed; moreover, several of the systems are substantially larger than the expected hydrodynamic screening length based on Koch and Shaqfeh theory, $\lambda \approx a/\phi=10a$. Thus it seems likely that these simulations contain sufficient particles to approximate the asymptotic large scale behavior of homogeneous suspensions, and provide a definitive answer to the question of the existence of hydrodynamic screening.

Instantaneous correlations in particle velocities decay in time due to the randomizing of particle positions by hydrodynamic diffusion. In Fig. 6, a typical set of velocity correlation functions ($N=7424$ and $a=2.443$) are compared with experimental data.⁶ The statistical errors in the simulated velocity correlation functions are quite small, of the order of 1% of the initial value, and less than the size of the plotting symbols; the statistical errors in the experimental data are much larger. The relaxation times are of the order $10t_0$, consistent with experimental observations,⁶ but the anisotropy in the simulated relaxation times $\tau_{\parallel}/\tau_{\perp} \approx 2.5$ is larger than ob-

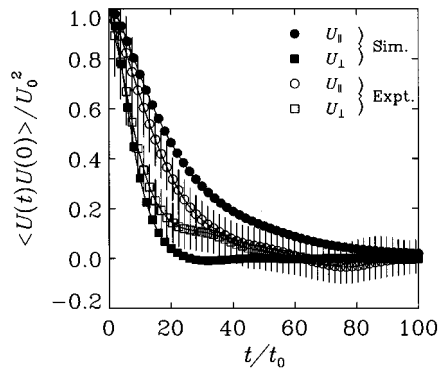


FIG. 6. Time-dependent velocity correlations. A typical set of velocity correlation functions ($a=2.443$, $N=7424$), normalized by the $t=0$ fluctuations, are plotted vs reduced time t/t_0 (solid symbols). The time scale $t_0=a/U_0$ is set by the time it takes an isolated sphere to fall a distance of one sphere radius. The open symbols are experimental data at the same volume fraction.

served experimentally ($\tau_{\parallel}/\tau_{\perp} \approx 1$). However it is in agreement with the theory for a random microstructure.¹⁴

The simulated relaxation times show a slow but steady increase with system size (Fig. 7). In the vertical direction, the simulated relaxation times are consistently larger than the experimental measurements. Assuming that the particle motion is diffusive and that the suspension microstructure is random, it is possible to calculate the relaxation times for dilute suspensions theoretically.¹⁴ The overall scaling of the relaxation times with system size is predicted to be proportional to \sqrt{W} for a random microstructure; this rather weak dependence, equivalent to $N^{1/6}$ for a constant aspect ratio box, is consistent with the simulations (Fig. 7).

The hydrodynamic dispersion coefficients $D = \langle U^2 \rangle \tau$ are plotted in Fig. 8. Once again, the data follows the theory for a random long-range microstructure ($D \propto W^{3/2}$), rather than showing evidence of a plateau value, which would be expected if hydrodynamic screening were occurring. Thus the simulations strongly suggest that both the velocity fluctuations and hydrodynamic diffusion coefficients diverge without bound in homogeneous suspensions. It should be noted that, for the largest system studied ($N=32\,768$), the vertical

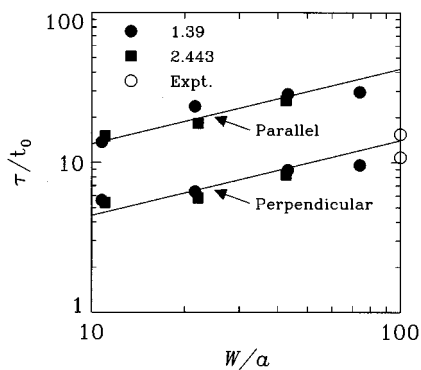


FIG. 7. Variation in velocity relaxation times (τ) with box size in a steadily sedimenting suspension. The solid line is the theoretical scaling ($\propto W^{1/2}$) for an equilibrium (most probable) distribution of spheres.¹⁴ The symbols have the same meaning as in Fig. 5.

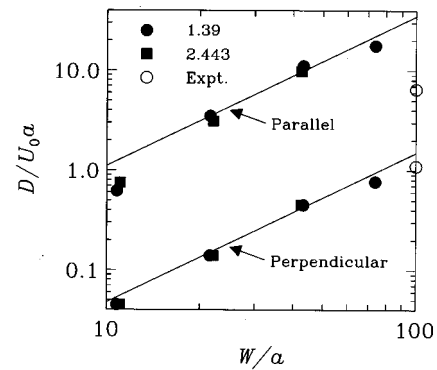


FIG. 8. Variation in hydrodynamic diffusion coefficients ($D = \langle U^2 \rangle \tau$) with box size in a steadily sedimenting suspension. The solid line is the theoretical scaling ($\propto W^{3/2}$) for an equilibrium (most probable) distribution of spheres.¹⁴ The symbols have the same meaning as in Fig. 5.

diffusion coefficient has already exceeded the experimental data by a factor of 2. As will be seen in the next section, our results rule out the possibility of a bulk hydrodynamic screening mechanism. It therefore seems that the experimental results can only be explained by explicitly including the effects of the container walls.

E. Structure

Significant changes in the short-range microstructure are induced by the sedimentation process. A comparison of pair correlations for most-probable and steady-state sedimentation microstructures is shown in Fig. 9. The large increase in pair correlations near contact is due to three-body hydrodynamic interactions.³ At somewhat larger separations, $5a < r < 15a$, the pair probability decreases more rapidly than for the most-probable distribution (see Fig. 10), perhaps by the mechanism suggested by Koch and Shaqfeh. However, it appears that the correlation times for the 3-body hydrodynamic interactions are not long enough to lead to sufficient deficit for hydrodynamic screening.

The mass deficit in a spherical shell around a test particle can be expressed in terms of the pair correlation function,

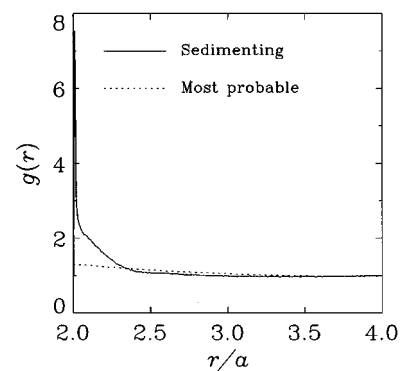


FIG. 9. Short-range pair correlations in a steadily sedimenting suspension. The steady-state pair correlation function from a typical sedimentation simulation ($a=2.443$, $N=7424$) is compared with the pair correlation function for the most-probable (equilibrium) distribution of spheres at the same volume fraction.

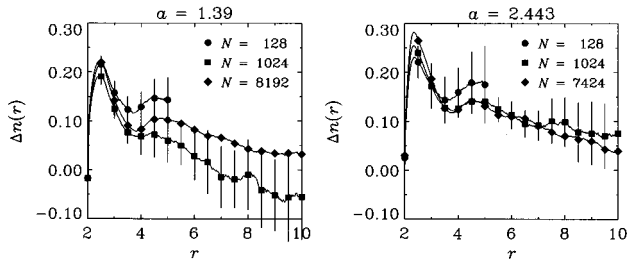


FIG. 10. Integrated pair correlations for different size systems. The quantity $n(r)$ measures the average deficit in the number of particles surrounding a test sphere; $\Delta n = n - n_{eq}$ is the difference between these quantities during steady-state sedimentation and for an equilibrium distribution. Results are plotted for different size systems as indicated in the figure; those on the left correspond to a particle radius $a = 1.39$ and those on the right to a particle radius $a = 2.443$. The statistical errors are indicated by the vertical bars.

$$n(r) = \frac{N}{V} \int_0^r [g(\mathbf{r}') - 1] d\mathbf{r}'. \quad (12)$$

In Fig. 10 the mass deficit for a sedimenting suspension is shown, relative to that for an equilibrium (most probable) distribution of spheres,

$$\Delta n(r) = n(r) - n_{eq}(r). \quad (13)$$

Results are shown for two different particle radii and three different system sizes for each particle radius. At small particle separations ($r < 3a$) there are quantitative differences between the pair correlation functions for different size particles, as can be seen by comparing the two plots in Fig. 10. However at large separations ($r \approx 10a$) there are no statistically significant differences in pair probability for the different size particles. Thus we can have confidence in the accuracy of the long-range pair correlations in simulations of large numbers of small particles ($a = 1.39$).

In order to test the validity of the Koch–Shaqfeh theory, the mass deficit $n(r)$ has been determined at distance scales larger than the expected screening length ($\lambda \approx 10a$ at $\phi = 0.1$); the results are shown in Fig. 11. There is some mass deficit even for the most-probable (or equilibrium) dis-

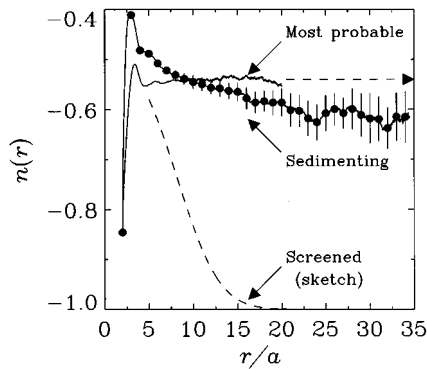


FIG. 11. Long-range pair correlations in sedimenting suspensions. The mass deficit, $n(r)$, is plotted for the largest simulated system $W \approx 70a$ ($a = 1.39$, $N = 32768$). The statistical errors are indicated by the vertical bars. The corresponding correlation function for the most probable distribution $n_{eq}(r)$ is also shown, together with a sketch of the correlation function predicted by the Koch–Shaqfeh theory.³

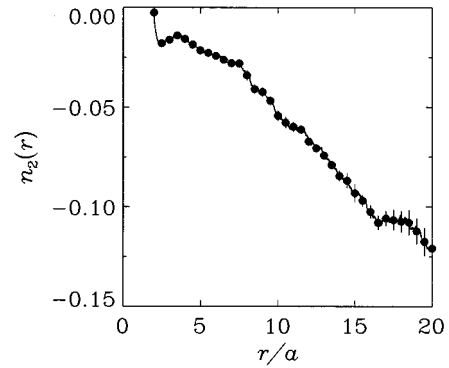


FIG. 12. Angle-dependent pair correlations in sedimenting suspensions. The average orientation of pairs of spheres relative to the direction of sedimentation, as measured by the second Legendre polynomial, is plotted as a function of r for a typical calculation ($a = 2.443$, $N = 7424$). The results indicate a slight preference for horizontal pairs.

tribution of non-overlapping spheres, $n_{eq}(r)$, because of excluded volume effects. However, the large- r asymptotic value of the deficit for the most-probable distribution is always greater than -1 ; at $\phi = 0.1$, $n_{eq}(r \rightarrow \infty) = -0.54$. By contrast, if there is hydrodynamic screening, then the Koch–Shaqfeh theory predicts that $n(r \rightarrow \infty)$ is exactly -1 . If the deficit is less than 1 particle or, in other words, if $n(r \rightarrow \infty) > -1$, there will not be a complete screening of the hydrodynamic interactions; the velocity fluctuations will diverge with a coefficient proportional to $1 + n(r \rightarrow \infty)$. Results for $n(r)$ from a numerical simulation of 32 768 sedimenting spheres are shown in Fig. 11. The pair correlation function is qualitatively different from what would be expected if there were hydrodynamic screening (shown by the dashed curve). It can be seen that $n(r)$ is essentially constant in the range $15a < r < 35a$; its large- r asymptotic value, $n(r \rightarrow \infty) = -0.6$, is close to that for the most-probable distribution.

The pair correlation function in a sedimenting suspension is not isotropic; there is a preferred direction, parallel to the gravitational force. The orientational anisotropy can be characterized by the second Legendre polynomial $P_2(\cos\theta)$, where θ is the angle between \mathbf{R}_{ij} and the gravitational field:

$$n_2(r) = \int_0^r g(\mathbf{r}') P_2(\cos\theta) d\mathbf{r}'. \quad (14)$$

The quantity $n_2(r)$, plotted in Fig. 12, is a measure of the directional preference of the pair correlation function. A large- r asymptotic limit of -0.5 would indicate that all pairs were horizontal, whereas an isotropic distribution would have $n_2 = 0$. Our results show a small but significant preference for a horizontal alignment of the pairs, as predicted by the Koch–Shaqfeh theory.³

V. CONCLUSIONS

We have computed pair correlation functions in steadily sedimenting suspensions out to large separations, well beyond the predicted screening length in Ref. 3. Our results do not show the mass deficit predicted by the Koch–Shaqfeh

theory. Although there are several possible sources of error in these simulations, it seems unlikely that these qualitative conclusions would be altered by more accurate calculations. On the other hand the indications of the beginning of a mass deficit in the isotropic pair correlation, together with the tendency of pairs to orient themselves horizontally, suggest that the three-body hydrodynamic interactions in the Koch–Shaqfeh theory are essentially correct. The most likely reason for the absence of the predicted mass deficit is that at typical volume fractions (i.e., $\phi > 0.01$) pairs of particles do not exist long enough for the screening mechanism to operate. This leaves open the possibility that a very dilute, perfectly monodisperse suspension could exhibit hydrodynamic screening, along the lines proposed by Koch and Shaqfeh. This possibility could be tested by large-scale Stokesian dynamics simulations.

The simulated velocity fluctuations and diffusion coefficients closely follow the theory for random dispersions¹⁴ and do not agree with experimental results, which show no system size dependence in either the velocity fluctuations or the diffusion coefficients.² These results suggest that other mechanisms must be uncovered to account for the experimental observations in Refs. 2 and 5.

From a computational point of view, the calculations represent an advance in the dynamical simulation of particle-fluid suspensions. Previous work⁹ was limited to samples of about 100 particles. The lattice-Boltzmann method, when implemented on a parallel computer can now simulate 10 000–100 000 particles, taking the full many-body hydrodynamic interactions into account.

ACKNOWLEDGMENTS

I would like to thank Don Koch (Cornell University) for many helpful and interesting discussions. I would also like to thank Elizabeth Guazzelli (ESPCI, Paris) for the experimental data used in Fig. 6. Much of this work was performed while I was on sabbatical leave at Cornell, in the Department of Theoretical and Applied Mechanics; my thanks to Jim

Jenkins and the TAM faculty for their hospitality. I would like to acknowledge generous allocations of computer time from the Livermore Computing Center and the Cornell Theory Center. This work was partially supported by the U.S. Department of Energy and Lawrence Livermore National Laboratory under Contract No. W-7405-Eng-48.

¹R. E. Caffisch and J. H. C. Luke, "Variance in the sedimentation speed of a suspension," *Phys. Fluids* **28**, 759 (1985).

²H. Nicolai and E. Guazzelli, "Effect of the vessel size on the hydrodynamic diffusion of sedimenting spheres," *Phys. Fluids* **7**, 3 (1995).

³D. L. Koch and E. S. G. Shaqfeh, "Screening in sedimenting suspensions" *J. Fluid Mech.* **224**, 275 (1991).

⁴A. J. C. Ladd, "Hydrodynamic screening in sedimenting suspensions of non-Brownian spheres," *Phys. Rev. Lett.* **76**, 1392 (1996).

⁵J. Z. Xue, E. Herbolzheimer, M. A. Rutgers, W. B. Russel, and P. M. Chaiken, "Diffusion, dispersion, and settling of hard spheres," *Phys. Rev. Lett.* **69**, 1715 (1992).

⁶H. Nicolai, B. Herzhaft, E. J. Hinch, L. Oger, and E. Guazzelli, "Particle velocity fluctuations and hydrodynamic self-diffusion of sedimenting non-Brownian spheres," *Phys. Fluids* **7**, 12 (1995).

⁷G. K. Batchelor, "Sedimentation in a dilute dispersion of spheres," *J. Fluid Mech.* **52**, 245 (1972).

⁸C. W. J. Beenakker and P. Mazur, "Is sedimentation container-shape dependent?," *Phys. Fluids* **28**, 3203 (1985).

⁹A. J. C. Ladd, "Dynamical simulations of sedimenting spheres," *Phys. Fluids A* **5**, 299 (1993).

¹⁰A. J. C. Ladd, "Numerical simulations of particulate suspensions via a discretized Boltzmann equation Part I. Theoretical foundation," *J. Fluid Mech.* **271**, 285 (1994).

¹¹A. J. C. Ladd, "Numerical simulations of particulate suspensions via a discretized Boltzmann equation Part II. Numerical results," *J. Fluid Mech.* **271**, 311 (1994).

¹²O. P. Behrend, "Solid–fluid boundaries in particle suspension simulations via the lattice-Boltzmann method," *Phys. Rev. E* **52**, 1164 (1995).

¹³G. K. Batchelor and J. T. Green, "The hydrodynamic interaction of two small freely-moving spheres in a linear flow field," *J. Fluid Mech.* **56**, 375 (1972).

¹⁴D. L. Koch, "Hydrodynamic diffusion in a suspension of sedimenting point particles with periodic boundary conditions," *Phys. Fluids* **6**, 2894 (1994).

¹⁵A. J. C. Ladd, "Hydrodynamic interactions in a suspension of spherical particles," *J. Chem. Phys.* **88**, 5051 (1988).

¹⁶A. J. C. Ladd, "Hydrodynamic transport coefficients of random dispersions of hard spheres," *J. Chem. Phys.* **93**, 3484 (1990).